

A compact model for electroosmotic flows in microfluidic devices

R Qiao¹ and N R Aluru^{2,3}

¹ Department of Mechanical and Industrial Engineering, University of Illinois at Urbana-Champaign, 405 N. Mathews mc 251, Urbana, IL 61801, USA

² Department of General Engineering, 3265 Beckman Institute for Advanced Science and Technology, University of Illinois at Urbana-Champaign, 405 N. Mathews mc 251, Urbana, IL 61801, USA

E-mail: aluru@uiuc.edu

Received 21 February 2002, in final form 23 May 2002

Published 21 June 2002

Online at stacks.iop.org/JMM/12/625

Abstract

A compact model to compute flow rate and pressure in microfluidic devices is presented. The microfluidic flow can be driven by either an applied electric field or a combined electric field and pressure gradient. A step change in the ζ -potential on a channel wall is treated by a pressure source in the compact model. The pressure source is obtained from the pressure Poisson equation and conservation of mass principle. In the proposed compact model, the complex fluidic network is simplified by an electrical circuit. The compact model can predict the flow rate, pressure distribution and other basic characteristics in microfluidic channels quickly with good accuracy when compared to detailed numerical simulation. Using the compact model, fluidic mixing and dispersion control are studied in a complex microfluidic network.

1. Introduction

Integrated microfluidic systems with a complex network of fluidic channels are routinely used for chemical and biological analysis and sensing [1, 2]. Microfluidic systems have recently attained great popularity because of the ease with which fluid flow can be controlled. Fluid flow in microchannels can be controlled by applying an electric field, pressure gradient or by a combined electric field and pressure gradient. Two important issues that microfluidic device designers would like to understand are the flow rate and pressure distribution within any microfluidic network. Detailed knowledge of pressure distribution within any channel is especially important as a pressure gradient can lead to significant sample dispersion leading to poor electrophoretic separation efficiency [2, 3].

A typical approach to understand fluid flow in microchannels is to perform detailed numerical simulations in two or three dimensions using the partial differential equations that describe microfluidic transport. Detailed numerical simulations can be very accurate; however, they

can be expensive and prohibitive. Microfluidic designers, who would like to quickly explore the design space before a device is fabricated, need design tools that are much faster compared to detailed numerical simulators. Compact models can be enormously useful to microfluidic designers to quickly evaluate new design concepts as they are simplified models, very fast compared to detailed numerical simulators, and yet they are accurate enough to capture the basic physical characteristics [4–6]. As compact models can be easily integrated into readily available circuit design software, compact models for microfluidic devices can enable seamless and rapid integration of microfluidic devices with micromechanical, microelectronic and other components on a chip [7, 8].

In this paper, we report on the development of a compact model for microfluidic devices that use either an electric field or a combined electric field and pressure gradient as driving forces. In the proposed compact model, the microfluidic network is represented by two electrical circuits—the first circuit is to compute the electric potential in the network because of the applied potential and the second circuit is to compute the pressure in the entire network. The compact model involves several simplifying

³ <http://www.staff.uiuc.edu/~aluru>

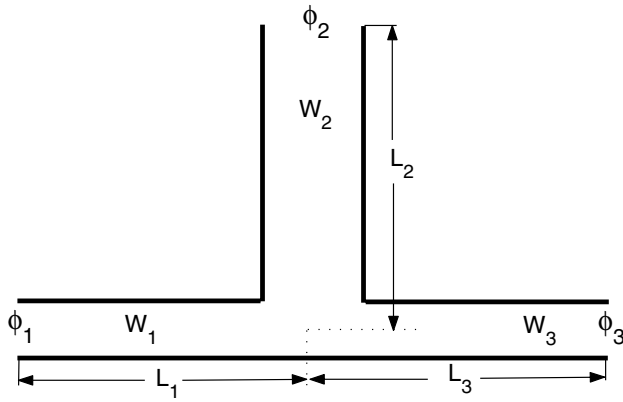


Figure 1. An applied potential field problem for a typical T-shape channel segment in a microfluidic system. The potentials ϕ_1 , ϕ_2 and ϕ_3 are given.

assumptions and the validity of the assumptions is discussed in detail. A novel aspect of the approach involves the treatment of a discontinuous change in the ζ -potential on the channel walls. Specifically, the discontinuous change in the ζ -potential is represented by a pressure source at the point of discontinuity. Numerical results indicate that the compact model can be several orders of magnitude faster compared to detailed numerical simulators without sacrificing too much accuracy.

The rest of the paper is organized as follows: section 2 describes the development of the compact model for microfluidic networks. Starting from detailed mathematical models, the compact model is derived and the underlying assumptions are clearly stated and discussed. The expression for a pressure source term to represent a discontinuous change in the ζ -potential variation is also derived. Section 3 gives several examples demonstrating the usefulness of the compact model. Finally, conclusions are presented in section 4.

2. Compact model development

The derivation of a compact model for a two-dimensional electroosmotic flow is described in this section. The approach can be extended in a straightforward manner when the flow is driven by other types of forces, e.g. a combined pressure gradient and an electric field. The compact model is composed of two parts, namely, the electrical part and the fluidic part.

2.1. Compact model: electrical part

For microfluidic devices that rely on electrokinetic force as the driving force, the electric field must be solved first. In the case of electroosmotic flow, the potential field due to an applied potential can be computed by solving the Laplace equation [9]:

$$\nabla^2 \phi = 0 \quad (1)$$

where ϕ is potential. To solve equation (1) on a complex geometry, the network of fluidic channels is represented by a number of straight channels and each straight channel is further represented as a resistor. For example, for the fluidic network shown in figure 1, the electrical part of the compact

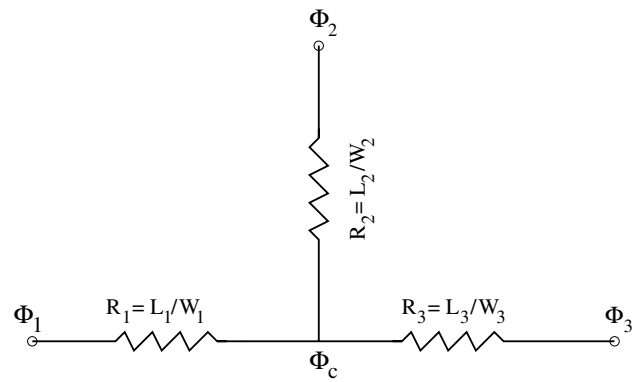


Figure 2. Electrical network representation for the applied potential field problem shown in figure 1.

model is represented by the circuit shown in figure 2. The resistance is defined by

$$R = \frac{L}{W} \quad (2)$$

where L is the channel length and W is the channel width (or cross-sectional area of the channel in the case of three-dimensional analysis). Assuming that the potential drops linearly in each straight channel and that the channel walls are well insulated, the applied potential field in the entire network is obtained by solving the circuit problem (see e.g. [10] for an electrical circuit approach to solve problems similar to the potential problem). In most microfluidic devices, the channel width is much smaller compared to the length of the channel. Hence, the assumption employed above is justified in most parts of the fluidic network except near channel intersections.

2.2. Compact model: fluidic part

The flow field in microfluidic devices is governed by the continuity equation (equation (3)) and the momentum equation (equation (4)) [9], i.e.,

$$\nabla \cdot \mathbf{u} = 0 \quad (3)$$

$$(\mathbf{u} \cdot \nabla) \mathbf{u} = \nu \nabla^2 \mathbf{u} - \frac{1}{\rho} \nabla p + \frac{1}{\rho} \mathbf{F}. \quad (4)$$

For electroosmotic flow, the body force term in equation (4) is obtained by solving the Poisson–Boltzmann equation

$$\nabla^2 \psi = \frac{1}{\lambda_D^2} \frac{RT}{F} \sinh \left(\frac{F\psi}{RT} \right) \quad (5)$$

$$\mathbf{F} = \epsilon \nabla \phi \nabla^2 \psi. \quad (6)$$

Equation (5) is the Poisson–Boltzmann equation for the ψ field induced by the ζ -potential on the channel wall and equation (6) is an expression for the body force term. Here R is the gas constant, F is the Faraday's constant, T is the temperature, ϵ is the permittivity of the fluid and λ_D is the Debye length defined by

$$\lambda_D = \left(\frac{\epsilon RT}{2F^2 c_0} \right)^{\frac{1}{2}} \quad (7)$$

where c_0 is the intrinsic ionic concentration of the fluid in the absence of a potential. Note that the body force term \mathbf{F} is

nonzero only within a few Debye lengths from the channel wall because the potential induced by the ζ -potential drops to zero very quickly near the channel wall [9]. We assume that the fluid properties (e.g. kinematic viscosity, ν) are uniform within the channel system.

In this paper we assume that: (1) the flow is fully developed in most parts of the channel system and (2) the effect of electrokinetic force can be represented by a slip velocity at the wall given by the Helmholtz–Smoluchowski equation [2]

$$u_{\text{slip}} = -\frac{\epsilon\zeta}{\mu}\nabla\phi \quad (8)$$

where μ is the dynamic viscosity of fluid.

The first assumption is justified because in typical microfluidic systems, the length of each channel segment is usually much longer compared to the channel width. However, for a nonuniform ζ -potential on the channel wall, the first assumption may not be valid in the regions where the ζ -potential changes. In fact, nonuniform ζ -potential on a channel wall can be observed in many circumstances, for example, when the channel is made from different materials in the axial direction [3] or when there is an applied electric field in the radial direction of the channel. In this paper, we assume that the ζ -potential changes in a discrete step manner, which is a good approximation when the nonuniformity of the ζ -potential is confined to a small region of the entire channel system.

The second assumption is justified because the electrokinetic force dominates the flow within the region which is a few Debye lengths from the channel wall, and the velocity of flow at the edge of the region can be approximated very well even if there is a small pressure gradient in the flow direction [11]. Since the thickness of the region is only a few nanometers, it is reasonable to assume that there is a slip velocity at the channel wall since the channel width is of the order of tens of micrometers.

Based on these assumptions, the velocity profile across a two-dimensional channel is a function of only the slip velocity and the pressure gradient, i.e.,

$$u_{\text{streamwise}} = -\frac{1}{2\mu}\frac{dp}{dx}\left(y^2 - \frac{h^2}{4}\right) + u_{\text{slip}} \quad (9)$$

where x denotes the stream-wise direction of the channel, y denotes the transverse direction across the channel and h is the channel width. With u_{slip} given by equation (8), solving for velocity is reduced to computing the pressure distribution in the fluidic network.

Typically, the pressure is strongly coupled with the velocity for incompressible flows. This can be seen by taking the divergence of the momentum equation (4) and applying the continuity equation (3),

$$\nabla^2 p = \nabla \cdot \mathbf{F} - \nabla \cdot (\rho(\mathbf{u} \cdot \nabla)\mathbf{u}). \quad (10)$$

In the regions where the flow is fully developed, the convection term $(\mathbf{u} \cdot \nabla)\mathbf{u}$ is zero, thus $\nabla \cdot (\rho(\mathbf{u} \cdot \nabla)\mathbf{u})$ vanishes. The term $\nabla \cdot \mathbf{F}$ must be zero in the fully developed flow regions, otherwise, the flow would not be fully developed due to the nonuniform body force. Thus, for the region where the flow is fully developed, the pressure calculation is reduced to a Laplace equation

$$\nabla^2 p = 0. \quad (11)$$

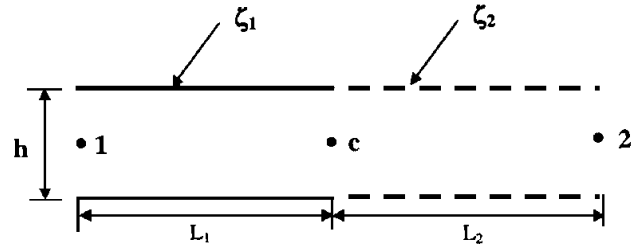


Figure 3. A channel with a discontinuous ζ -potential change at point c . The ζ -potential change at point c is represented by a pressure source in the compact model.

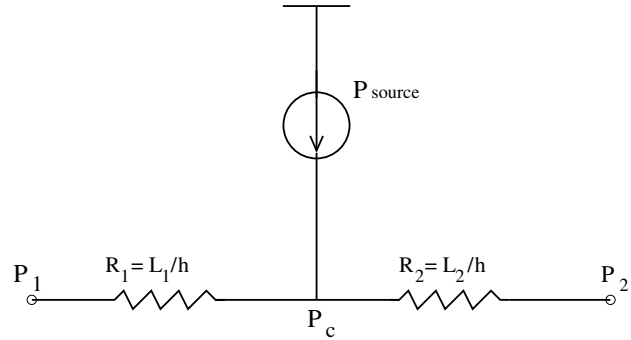


Figure 4. Electrical network representation of pressure field problem shown in figure 3. P_1 , P_2 and P_c are the pressure at points 1, 2 and c , respectively. P_{source} is the pressure source that is applied to treat the discontinuous change in the ζ -potential.

Observe that equation (11) decouples the solution of pressure from the solution of velocity.

For regions where the ζ -potential on the channel wall is not uniform, the source term on the right-hand side of equation (10) is not zero. In general, it cannot be calculated before the velocity is known. However, with the assumption that the flow is fully developed everywhere except in the regions where the ζ -potential on the channel wall is not uniform, one can estimate the right-hand side source term in equation (10) by using the mass conservation principle. Once the source term is known, one can solve for the pressure by setting up an electrical network representing the fluidic system. For example, consider a straight channel consisting of two different regions of ζ -potential on the wall (see figure 3). The ζ -potential for the channel region with length L_1 is ζ_1 , and the ζ -potential for the channel region with length L_2 is ζ_2 . The ζ -potential is assumed to change discontinuously from ζ_1 to ζ_2 at point c . The pressure calculation for this example can be represented by the electrical network shown in figure 4. Because there is a step change of ζ -potential on the wall at point c , the source term (right-hand side of equation (10)) is nonzero, and this is represented by the pressure source term in figure 4. Since we assume that the flow is fully developed everywhere (except near point c), the velocity u and flow rate q are given by

$$u = \frac{1}{2\mu}\frac{\Delta P}{\Delta X}\left(y^2 - \frac{h^2}{4}\right) + u_{\text{slip}} \quad (12)$$

$$q = u_{\text{slip}}h - \frac{1}{12\mu}\frac{\Delta P}{\Delta L}h^3 \quad (13)$$

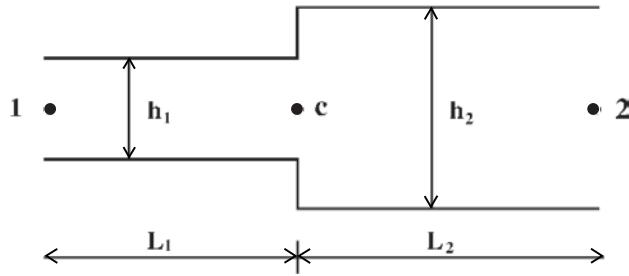


Figure 5. A channel with a discontinuous channel width at point c . The channel width change at point c is represented by a pressure source in the compact model.

where h is the width of the channel and u_{slip} is the slip velocity at the channel wall calculated from equation (8). Since we assume that the flow is fully developed, the pressure drops linearly along the channel except near point c . Thus, integration of the pressure Poisson equation (equation (10)) in the entire channel yields

$$\frac{(P_c - P_1)h}{L_1} + \frac{(P_c - P_2)h}{L_2} = P_{\text{source}}. \quad (14)$$

Equating the flow rate in the left and right parts of the channel and applying equation (14) gives

$$P_{\text{source}} = 12\mu \frac{u_{\text{slip},L_1} - u_{\text{slip},L_2}}{h} \quad (15)$$

where u_{slip,L_1} and u_{slip,L_2} are the slip velocities on the channel walls in channel regions denoted by L_1 and L_2 , respectively.

It is straightforward to set up an electrical circuit for more complex fluidic systems to compute pressure at every point in the channel system. Once the pressure is computed, the flow rate can be obtained by using equation (13).

Though the above derivation is for a two-dimensional channel system, the development can be extended to three-dimensional channel systems very easily. The derivation is valid even if the cross-section of the channel is irregular because it has been shown that for a fully developed flow in a straight channel of arbitrary shape, the flow rate can always be expressed as

$$Q = -\frac{dP}{dX} f \quad (16)$$

where f is a function whose value is related to the shape of the cross-section of the channel only, and can be obtained either analytically for simple cross-sectional shapes [12] or from numerical simulations for more complex shapes. Once f is known, P_{source} can be determined by the approach described above. For example, if the channel shown in figure 3 has a circular cross-section, the pressure source term can be expressed as

$$P_{\text{source}} = 8\pi\mu (u_{\text{slip},L_1} - u_{\text{slip},L_2}). \quad (17)$$

Remarks. Instead of a step change in the ζ -potential, if there is a step change in the channel width in a fluidic system, the pressure distribution can be computed by setting up an electrical network similar to that shown in figure 4. For example, for the two-dimensional channel shown in figure 5, the corresponding electrical network is identical to the network shown in figure 4. To compute the pressure source term, once

again we equate the flow rate in the left and right parts of the channel. Using equation (14), the pressure source term is found to be

$$P_{\text{source}} = \left(\frac{\frac{h_1}{L_1} + \frac{h_2}{L_2}}{1 + \frac{L_1}{L_2} \left(\frac{h_2}{h_1} \right)^3} - \frac{h_1}{L_1} \right) P_1 + \left(\frac{\frac{h_1}{L_1} + \frac{h_2}{L_2}}{1 + \frac{L_2}{L_1} \left(\frac{h_1}{h_2} \right)^3} - \frac{h_2}{L_2} \right) P_2. \quad (18)$$

3. Numerical examples

3.1. Validation of compact model

In the derivation of the compact model, it has been assumed that the flow is fully developed in most of the channel systems and the slip velocity is given by equation (8) at the channel wall. Though these assumptions can be justified in simple fluidic systems, it is important to evaluate the accuracy of the compact model based on these assumptions when applied to complex fluidic systems. Figure 6 shows a typical microfluidic network that can be used for fluidic transport or other purposes. The ζ -potential on the left half (all channel walls to the left of the dashed line in figure 6) and on the right half of the fluidic network is -10 mV and -30 mV, respectively. The flow rate in each segment of the channel system is controlled by varying the applied potential at reservoirs 0, 1, 2, 3, 4 and 5. In some cases, where pressure driven flow is more desirable [13], the flow rate can also be controlled by varying the pressure at these reservoirs. To investigate the accuracy of the compact model developed here, two test problems have been tried for the channel system shown in figure 6. The first test case is an electroosmotic flow and the second test case is a combined electroosmotic and pressure driven flow.

3.1.1. Electroosmotic flow case. In the first test case, the pressure at all the reservoirs is set to zero. A potential of 100 V is applied at reservoirs 0, 1 and 2 and a potential of 60 V is applied at reservoir 3. All other reservoirs are grounded. Both full simulation (two dimensional) based on Navier–Stokes equations and compact model analysis have been performed for the fluidic network. In the full simulation, two cases with different Debye lengths (λ_D) have been investigated: $\lambda_D = 1.25 \mu\text{m}$ and $\lambda_D = 2.50 \mu\text{m}$. Note that the actual Debye length is of the order of tens of nanometers and cannot be resolved in a full simulation, so a much larger Debye length (typically a few microns) is typically used in numerical simulations. The justification for this can be found in a previous paper [9]. The Reynolds number based on average velocity for cross-section 0 to 7 (see figure 6) are 0.032, 0.016, 0.027, 0.047, 0.056, 0.065, 0.074 and 0.12, respectively, for $\lambda_D = 1.25 \mu\text{m}$.

The full simulation involves the solution of the Laplace equation (equation (1)) for the applied potential, the Poisson–Boltzmann equation (equation (5)) for the ζ -potential, and the momentum (equation (4)) and continuity equation (equation (3)) for fluid flow. Detailed algorithms can be found in [9]. The viscosity (ν) and permittivity (ϵ) of the fluid are set to be $10^{-6} \text{ m}^2 \text{ s}^{-1}$ and $6.95 \times 10^{-10} \text{ C}^2 \text{ J}^{-1} \text{ m}^{-1}$, respectively.

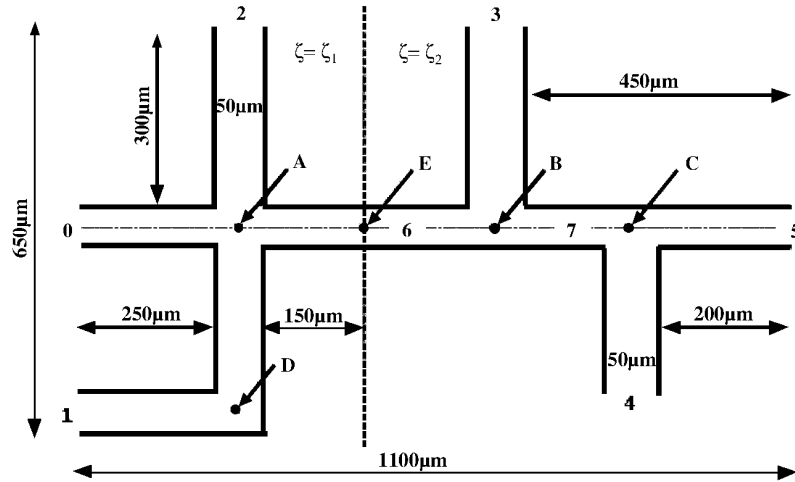


Figure 6. A typical microfluidic network. All the channels have the same width of $50 \mu\text{m}$.

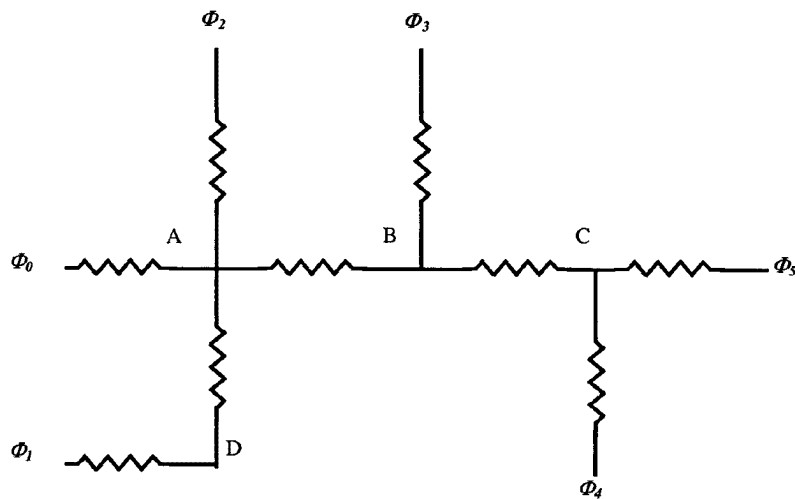


Figure 7. A circuit model to compute the potential distribution for the microfluidic network shown in figure 6.

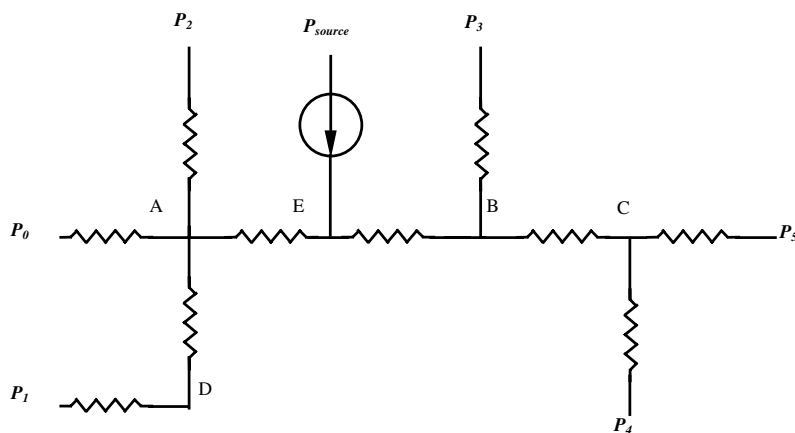


Figure 8. A circuit model to compute the pressure distribution for the microfluidic network shown in figure 6.

The same values of ν and ϵ are used for all the other examples discussed in this paper. The channel system is discretized into 5838 and 8154 points for $\lambda_D = 2.50 \mu\text{m}$ and $\lambda_D = 1.25 \mu\text{m}$, respectively. The total number of unknowns (ϕ , ψ , \mathbf{u} and P) for the two cases are 29190 and 40770, respectively. In

the compact model analysis, a circuit model (see figure 7) to compute the applied potential distribution in the channel system and a circuit model (see figure 8) to compute the pressure distribution in the channel system are set up based on the method presented in sections 2.1 and 2.2. The total

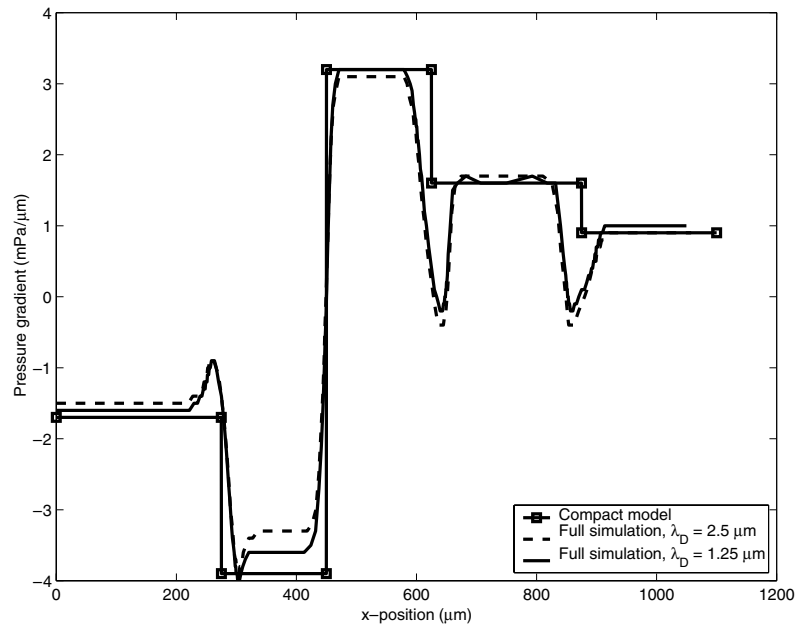


Figure 9. Comparison of pressure gradient along the line 0–A–C–5 in figure 6 obtained by the compact model and full simulation.

number of unknowns in the compact model is only 9 ($\phi_A, \phi_B, \phi_C, \phi_D, P_A, P_B, P_C, P_D$ and P_E). Clearly, the computational cost of the compact model is negligible compared to that of the full simulations.

When there is a discontinuity of ζ -potential on the channel wall in a fluidic network, it is important to know the pressure distribution (or more precisely, the pressure gradient) in the fluidic network because the flow caused by the pressure gradient can cause hydrodynamic dispersion which is detrimental to certain applications such as electrophoretic separation. Figure 9 shows the comparison of the pressure gradient along the line 0–A–C–5 (see figure 6) obtained by full simulation and the compact model. For locations far away from the channel intersections, the compact model prediction deviates slightly from the full simulation results (the error is quite small and is within 8%). It is also observed that such a deviation decreases as the Debye length is decreased in the full simulation. Because the Debye length in actual microfluidic devices is much smaller than the values used in the full simulation, it is expected that the compact model can predict the pressure distribution in microfluidic networks with good accuracy. It can be seen from figure 9 that the compact model cannot capture the pressure variation near channel intersections very well. The reason for such discrepancy is the assumptions made in the compact model that are not valid near channel intersections. Specifically, the flow is not fully developed near channel intersections and the pressure distribution is complicated. To capture such a complicated flow pattern, the Navier–Stokes equations must be solved in the region.

Figure 10 shows the scaled error in the flow rate at different positions of the network and the compact model provides a solution that is within 8% accuracy when λ_D/W is 0.05 and within 3% accuracy when λ_D/W is 0.025. From figures 9 and 10, it can be observed that the compact model gives better results when the λ_D/W ratio is small. This is because as the

λ_D/W ratio decreases, the slip velocity model becomes more accurate. Since the Debye length usually ranges from a few nanometers to tens of nanometers in microfluidic devices (i.e. the λ_D/W ratio is typically in the order of 10^{-5} to 10^{-3}), the compact model proposed in this paper can be expected to provide high accuracy results for microfluidic networks.

3.1.2. Combined electroosmotic and pressure driven flow case. The applied potentials for this test case are identical to the potentials applied for the electroosmotic flow test case discussed in section 3.1.1. However, the pressure at reservoir 0 is set to 3 Pa, and the pressure at all other reservoirs is set to zero. This is a more complex scenario compared to the first problem, because in this problem, the pressure gradient in the channel is due to the pressure induced by the nonuniform ζ -potential on the channel wall as well as due to the applied pressure at reservoirs. Full simulation and compact model analysis were performed for this problem. Figure 11 shows the pressure gradient along the line 0–A–C–5 in figure 6. It indicates that the compact model can predict the pressure gradient in the system when there are multiple sources for pressure gradient in the channel. Figure 12 shows the comparison of velocity profile obtained by full simulation and the compact model at cross-sections 0 and 5 (see figure 6 for the location of these cross-sections). It shows that the compact model can predict the velocity fairly accurately except very near the wall.

3.2. Application of the compact model to a complex microfluidic network

As the compact model can compute the flow rate and pressure distribution in a microfluidic system very efficiently, it could be very useful when searching for an appropriate control strategy for a fluidic system.

Figure 13 shows a microfluidic network that can be used for fluid mixing and separation. The radius of the

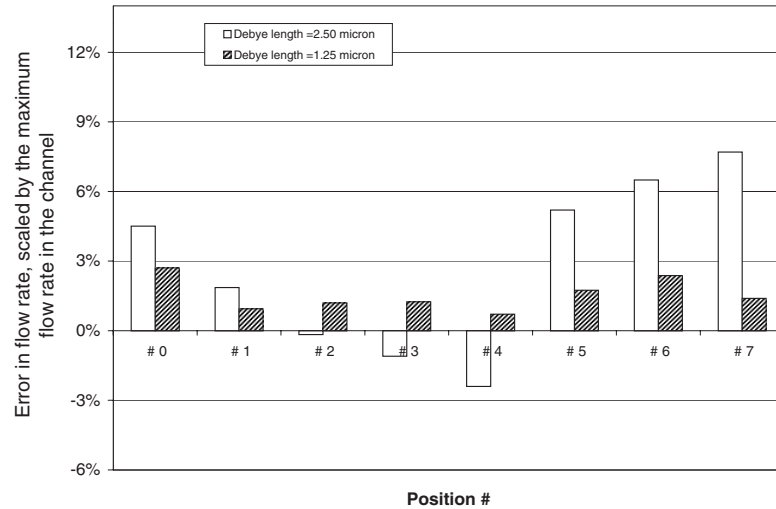


Figure 10. Scaled error in flow rate computed by the compact model for the various positions shown in figure 6.

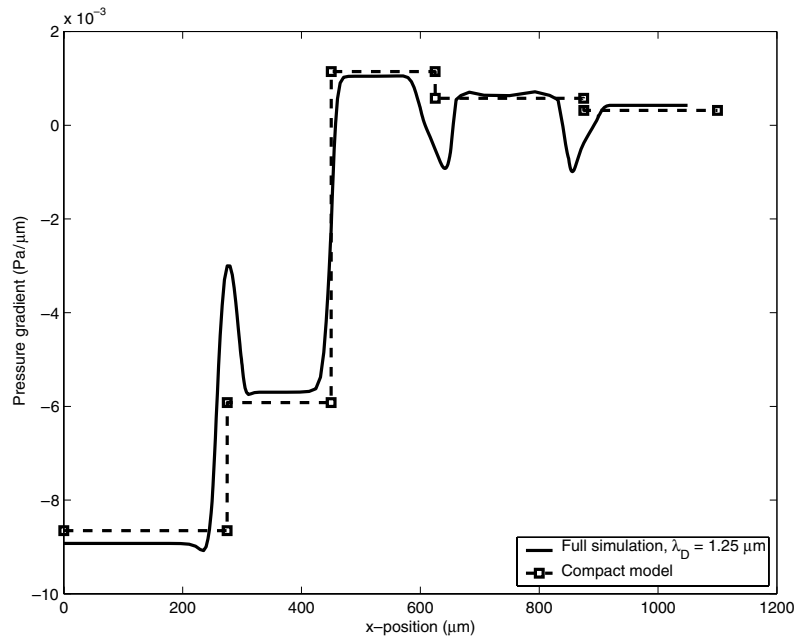


Figure 11. Comparison of pressure gradient along the line 0–A–C–5 in figure 6 obtained by the compact model and full simulation.

circular cross-section channel is $50 \mu\text{m}$. The length of the channel regions $o-a$, $o-b$, $o-d$, $a-c$, $b-e$ and $d-f$ are 0.5 mm, 0.5 mm, 3 mm, 1 mm, 1.5 mm and 0.49 mm, respectively. The fluidic network is symmetrical with respect to the axis $e-b-o-d$. With an appropriate potential applied at reservoirs 1, 2 and 3 (reservoir 4 is always grounded), fluid A will flow from reservoirs 1 and 3 towards reservoir 4 and fluid B will flow from reservoir 2 towards reservoir 4. We present two examples here to illustrate how the compact model can be used to search for an appropriate control strategy for this microfluidic system.

3.2.1. Fluid mixing. On-chip dilution and mixing of fluids in microfluidic devices have been demonstrated successfully by the use of both electrokinetic force and pressure gradient

[1, 13]. Using electrokinetic forces has the advantage of simplicity and quick response. However, it has been shown that electroosmotic flow depends strongly on the surface properties of the channel, which can make the flow control quite difficult. For example, when the ζ -potential on the channel walls is uniform in the entire channel system, the velocity at any position in the channel can be obtained by the similitude between the electric field and the flow field. But, when there is a nonuniform ζ -potential on the channel walls, such similitude is not applicable and the calculation of flow rate can become difficult. In this case, the compact model developed in this paper can be used to analyze the flow rate at various positions in the system efficiently.

For the fluidic system shown in figure 13, there are three different ζ -potentials on the channel walls due to the different properties of fluid in the channel. We assume that the various

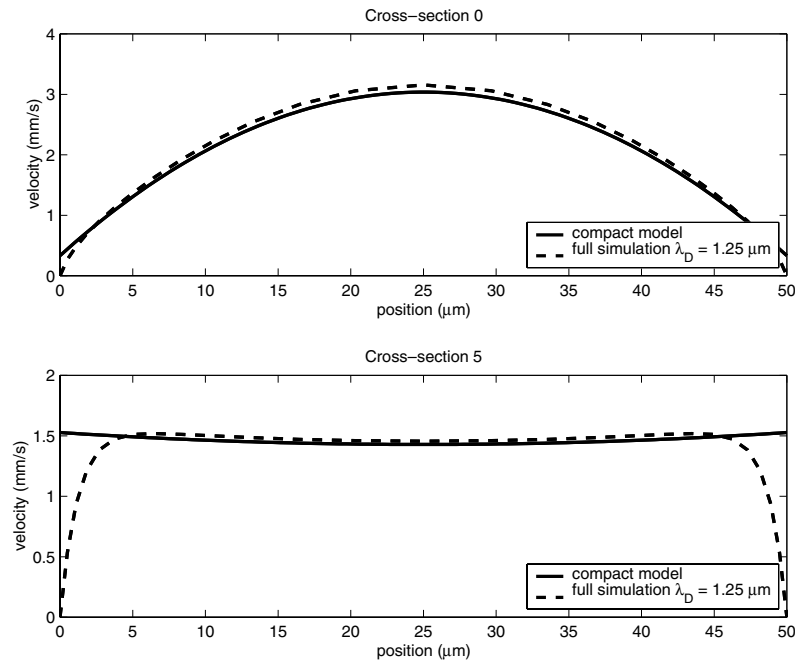


Figure 12. Comparison of velocity profile obtained by the compact model and full simulation at cross-sections 0 (top) and 5 (bottom). See figure 6 for the location of cross-sections 0 and 5.

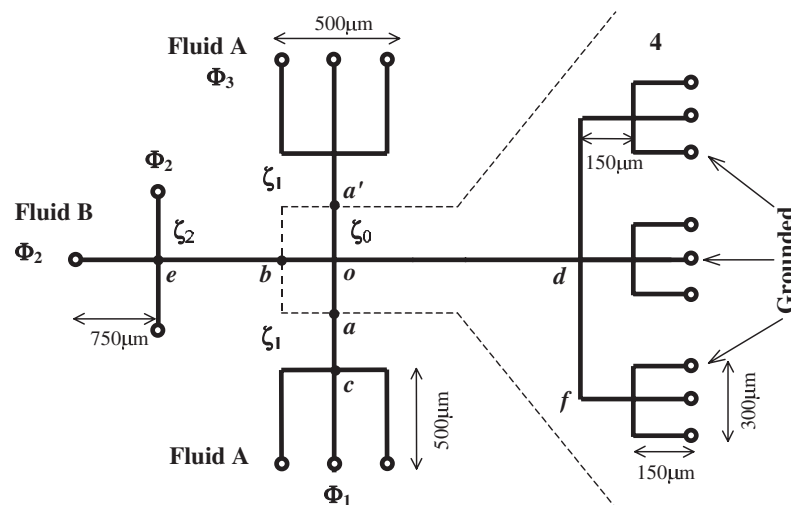


Figure 13. A microfluidic network for mixing and separation. The dotted line denotes the region where the ζ -potential is ζ_0 . Observe that the ζ -potential changes from ζ_2 to ζ_0 at point b and from ζ_1 to ζ_0 at points a and a' (figure not to scale).

ζ -potentials are given by $\zeta_1 = -70$ mV, $\zeta_2 = -30$ mV and $\zeta_0 = -20$ mV. Note that the ζ -potentials on the channel walls $o-b$, $o-a$ and $o-d'$ are assumed to be $\zeta_0 = -20$ mV. Figure 14 shows the circuit model to compute the pressure distribution in the channel system. The pressure source terms can be computed by using equation (17). Figure 15 shows how the ratio of flow rate of fluid A to fluid B (referred to as mixing ratio of A to B) in channel $o-d$ can be controlled by varying the potential applied at reservoir 2. Note that the total flow rate in channel $o-d$ is fixed at 3.6 nL s^{-1} and the potentials at reservoirs 1 and 3 are set to the same value. Figure 15 also shows the potential one needs to apply at reservoirs 1 and 3 so that the flow rate in channel $o-d$ is fixed at 3.6 nL s^{-1} . For any desired mixing ratio of A to B, one

can find the suitable potential at reservoirs 1 and 2 very easily. For example, for a mixing ratio of 1.5, the applied potential at reservoir 2 should be 120.5 V and that at reservoirs 1 and 3 should be 99.75 V to maintain a fixed flow rate of 3.6 nL s^{-1} in channel $o-d$.

3.2.2. Dispersion control. It has been shown that a nonuniform ζ -potential on the channel wall can result in serious deterioration of separation efficiency because the induced pressure gradient in a channel can cause significant sample dispersion [2, 3]. The sample variance caused by a pressure driven flow in a long circular pipe is given by [14]:

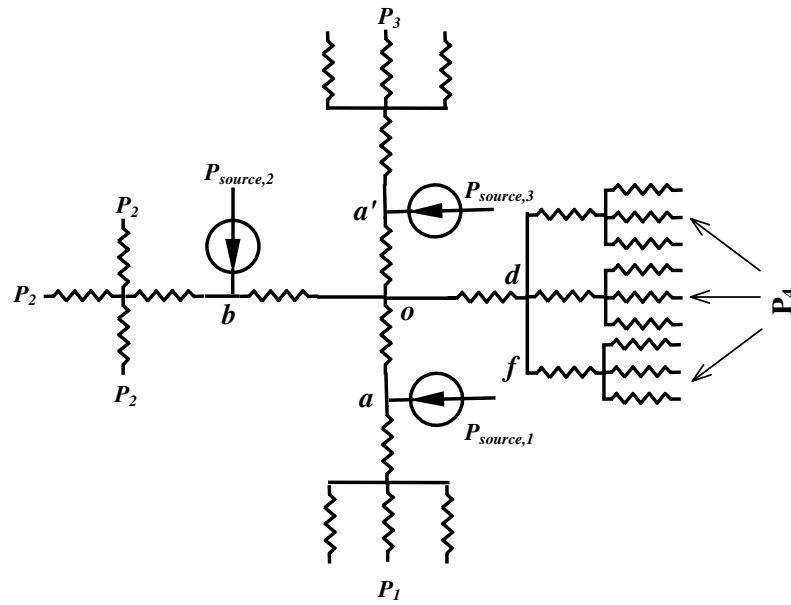


Figure 14. A circuit model to compute the pressure distribution for the fluidic network shown in figure 13.

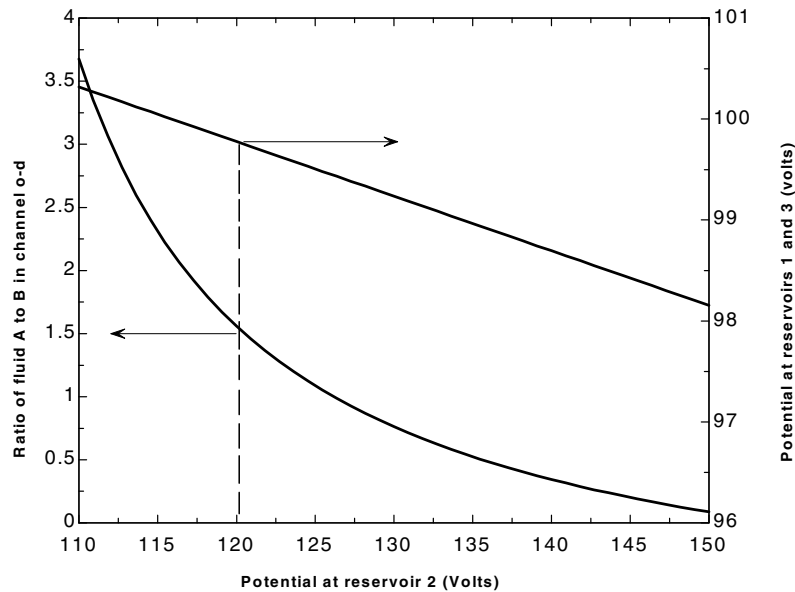


Figure 15. Control of the flow rate of fluids A and B in channel $o-d$ by varying the potential at reservoir 2. Total flow rate in channel $o-d$ is fixed at 3.6 nL s^{-1} . The appropriate potential at reservoirs 1 and 3 ($V_1 = V_3$) is computed by the compact model.

$$\sigma^2 = 2Dt + 2 \left(\frac{r^2 \bar{U}_{\text{pressure}}^2}{48D} \right) t \quad (19)$$

where D is the diffusion coefficient, r is the channel radius and $\bar{U}_{\text{pressure}}$ is the average velocity across the channel caused by the pressure gradient. The second term on the right-hand side of equation (19) denotes the hydrodynamic dispersion caused by the nonuniform velocity across the channel.

To study dispersion control, we again consider the fluidic network shown in figure 13. The ζ -potentials on the channel walls are as described in section 3.2.1. Because of the nonuniform ζ -potential on the channel walls in the microfluidic system (see figure 13), the pressure gradient

in channel $o-d$ is generally not zero, indicating that there would be hydrodynamic dispersion if channel $o-d$ is used as a separation channel. However, by controlling the pressure at reservoir 4, it is possible to minimize the pressure gradient in channel $o-d$, therefore minimizing the hydrodynamic dispersion in channel $o-d$. Assuming that the sample variance at point o in figure 13 is zero, and that the sample diffusion coefficient is $1.0 \times 10^{-10} \text{ m}^2 \text{ s}^{-1}$, figure 16 shows how the dispersion of the sample in channel $o-d$ (i.e. the sample variance σ^2 at point d in figure 13) can be controlled by varying the pressure at reservoir 4. Note that the applied potential at reservoir 2 is set to be 200 V and the ratio of fluid A to fluid B in channel $o-d$ is set to be 2:1. To maintain such a ratio,

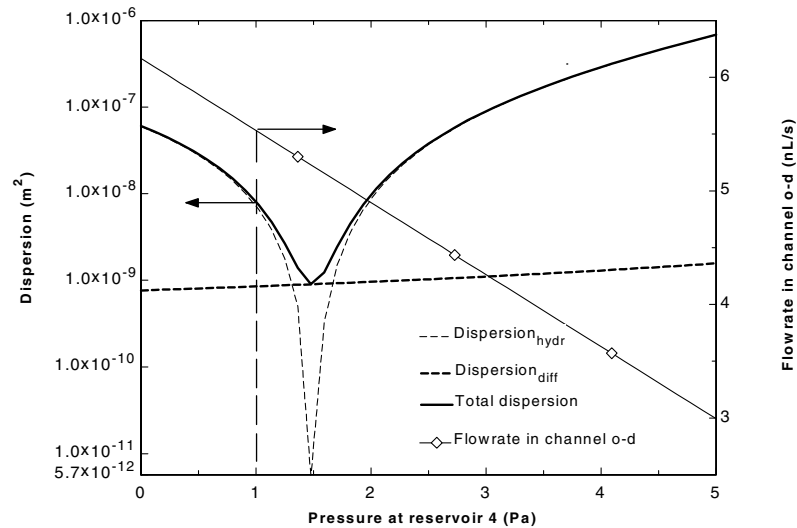


Figure 16. The dispersion of species in channel $o-d$ can be minimized by varying the pressure at reservoir 4. The applied potential at reservoir 2 is 200 V and the ratio of fluid A to B in channel $o-d$ is set to be 2:1. The appropriate potential at reservoirs 1 and 3 ($V_1 = V_3$) is computed by the compact model (see figure 17).

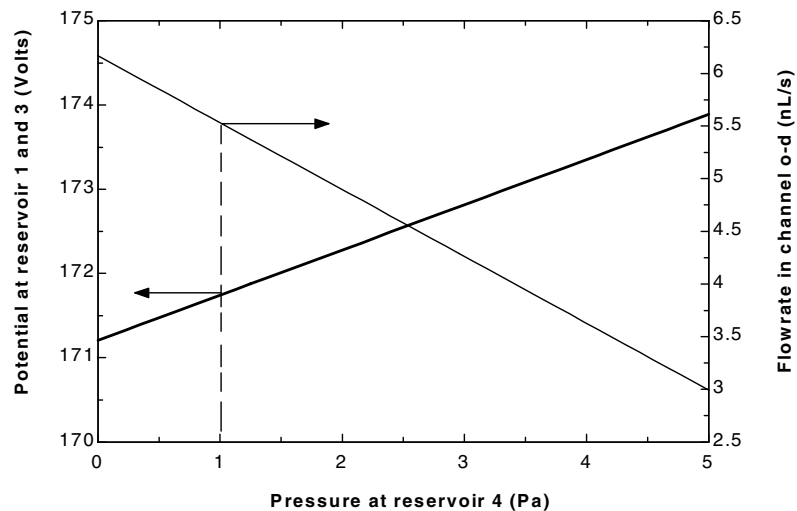


Figure 17. For any pressure applied at reservoir 4, the compact model computes the appropriate potential that needs to be applied at reservoirs 1 and 3 ($V_1 = V_3$) such that the ratio of fluid A and fluid B in channel $o-d$ is fixed at 2:1. The applied potential at reservoir 2 is maintained at 200 V. The flow rate (shown on the right y-axis) in channel $o-d$ is also calculated.

an appropriate potential must be applied at reservoirs 1 and 3 ($V_1 = V_3$). As shown in figure 17, when the pressure at reservoir 4 is varied, V_1 and V_3 are computed by the compact model. From figure 16, it can be seen that the flow rate (shown on the right y-axis in the figure) in channel $o-d$ decreases when the pressure at reservoir 4 is increased, indicating that the average velocity in the channel is lowered. This will result in a longer time for the sample to pass through the channel. Thus, the dispersion due to the diffusion (shown as $\text{Dispersion}_{\text{diff}}$ in figure 16) will increase. However, the dispersion due to the hydrodynamic effect (shown as $\text{Dispersion}_{\text{hydr}}$ in figure 16) will reach zero when the pressure at reservoir 4 is 1.49 Pa. The overall effect is that the total dispersion reaches a minima when the pressure at reservoir 4 is 1.489 Pa. The minimal dispersion is about two orders of magnitude lower than the original dispersion when the pressure at reservoir 4 is zero.

In practice, choosing the pressure at reservoir 4 can be a compromise between throughput (i.e. flow rate in channel $o-d$) and separation resolution.

4. Conclusion

A compact model for rapid analysis of electroosmotic flow in microfluidic devices and networks is presented. The compact model can analyze the flow rate and pressure distribution in a fluidic network when the driving force is either an electric field or a combined electric field and pressure gradient. The results obtained from the compact model are in good agreement with full simulation results. Compared to the full simulation, the compact model involves negligible computational cost. Detailed studies on fluidic mixing and dispersion control have been performed on a microfluidic network using the compact

model. As the fluidic network is represented by an electrical circuit in the compact model, the compact model can be easily integrated into readily available circuit analysis software.

References

- [1] Jacobson S C, McKnight T E and Ramsey J M 1999 Microfluidic devices for electrokinetically driven parallel and serial mixing *Anal. Chem.* **71** 4455–9
- [2] Probstein R F 1994 *Physicochemical Hydrodynamics* (New York: Wiley)
- [3] Herr A E, Molho J I, Santiago J G, Mungal M G, Kenny T W and Garguilo M G 2000 Electroosmotic capillary flow with nonuniform zeta potential *Anal. Chem.* **72** 1053–7
- [4] Vandermeer J E, Kanz M S and Fedder G K 1998 Hierarchical representation and simulation of micromachined inertial sensors *Technical Proc. 1998 Int. Conf. on Modeling and Simulation of Microsystems (Santa Clara, CA, April 1998)* pp 450–5
- [5] Wu J and Carley L R 2001 Table-based numerical macromodeling for MEMS devices *Technical Proc. 2001 Int. Conf. on Modeling and Simulation of Microsystems (Hilton Head Island, SC, March 2001)* pp 68–71
- [6] Casinovi G 2001 Efficient simulation of MEMS using element stamps *Technical Proc. 2001 Int. Conf. on Modeling and Simulation of Microsystems (Hilton Head Island, SC, March 2001)* pp 112–5
- [7] Kirby R K, Karniadakis G E, Mikulchenko O and Mayaram K 2001 An integrated simulator for coupled domain problems in MEMS *J. Microelectromech. Syst.* **10** 379–91
- [8] Mukherjee T and Fedder G K 1998 Design methodology for mixed-domain systems-on-a-chip *Technical Proc. 1998 IEEE Computer Society Workshop on VLSI (Orlando, FL, April 1998)* pp 96–101
- [9] Mitchell M, Qiao R and Aluru N 2000 Meshless analysis of steady-state electro-osmotic transport *J. Microelectromech. Syst.* **9** 435–49
- [10] Incopera F P and DeWitt D P 1996 *Fundamentals of Heat and Mass Transfer* (New York: Wiley)
- [11] Santiago J G 2001 Electroosmotic flows in microchannels with finite inertial and pressure forces *Anal. Chem.* **73** 2353–65
- [12] White F M 1991 *Viscous Fluid Flow* (New York: McGraw-Hill)
- [13] Chien Ring-Ling and Parce J W 2001 Multiport flow-control system for lab-on-a-chip microfluidic devices *Fresenius' J. Anal. Chem.* **371** 106–11
- [14] Taylor G 1953 Dispersion of soluble matter in solvent flowing slowly through a tube *Proc. R. Soc. A* **219** 186–203